36th EPS Conference on Plasma Phys. Sofia, June 29 - July 3, 2009 ECA Vol.**33E**, P-4.212 (2009)

Localisation and spatial resolution of the ECE diagnostic system for W7-X

S. Schmuck, H. J. Hartfuss, M. Hirsch
Max-Planck-Institut für Plasmaphysik EURATOM Association,
Wendelsteinstraße 1, D-17491 Greifswald, Germany

abstract: The stellarator Wendelstein 7-X (W7-X) under construction in Greifswald, Germany offers good conditions for ECE observation, i.e. the possibility for observation from both the low- (LFS) and high-field-sides (HFS) along the same line of sight. The LFS observation allows for electron temperature profile measurements with good spatial and temporal resolution. The back-end is a multichannel heterodyne radiometer. The radial resolution of the ECE system is being evaluated. Refraction, relativistic down-shift, radiation transport through the plasma and the instrumental resolution, as determined by the bandwidth of the individual filters of the filter bank in the radiometer back-end, are considered.

keywords: ECE diagnostics, localisation, spatial resolution, emission layer width

1 Introduction

At W7-X the basic condition for ECE diagnostics, i.e. a monotonously decreasing magnetic field along the line of sight, is fullfilled, thus allowing for measurements of the electron temperature profile [1]. To minimize Doppler-shift and refraction effects, the chosen line of sight is almost perpendicular to the magnetic field and the flux surface gradient. The main components are the Gaussian beam telescope and a multichannel heterodyne radiometer [2,3], measuring the ECE in the frequency range 126-162 GHz in second harmonic X-mode polarization (X2). The Gaussian beam telescope ensures a slim observation beam along the line of sight independent on frequency. Outside the ECE is guided by oversized waveguides about 40 m in length through the torus hall to the heterodyne radiometer. The ECE is down-converted to an intermediate frequency (IF) range of 4-40 GHz, covered by a 32 channel filter bank with center frequencies between 4.4-39.6 GHz and filter bandwidths 0.3-1.4 GHz. The power within the bands is detected by Schottky-diodes. In case W7-X is operated at reduced magnetic field (about 1.9 T on magnetic axis), the radiometer front-end coverage will be extended to cover the band from 90 GHz on. The collecting optics are designed, such that both X- and O-mode can be detected simultaneously. With both the HFS and LFS ECE spectrum available, information about the electron velocity distribution function can be gained [4]. The determination of the T_e profile includes the localisation and spatial resolution. Both are mandatory for integrated data analysis and plasma equilibrium reconstruction. In this paper our approach of the localisation and spatial resolution is described and demonstrated for two sets of plasma conditions at W7-X.

2 Localisation and spatial resolution

The multichannel radiometer measures the ECE intensity due to the absolute calibration (hot-cold source technique) in terms of the radiation temperature T_{Rad}. For optically thick plasmas, T_{Rad} approaches the electron temperature T_e. To obtain the electron temperature profile, a location has to be assigned to each channel representing the emission layer. The finite spatial width of the layer, determining the spatial resolution of the ECE diagnostic, can be determined in various approximations.
In a most simple approach, for the given magnetic field $B(R)$ along the radiometer line of sight and second harmonic observation, the cold resonance location R^i_{CR} is assigned to the ith channel with center

frequency f^i_{CF}, considering relativistic corrections by the measured radiation temperature T^i_{Rad}, via

$$B(R^i_{CR}) = m_{e0}\pi f^i_{CF}/(e\sqrt{1 - k_B T^i_{Rad}/m_{e0}c^2}) \quad . \tag{1}$$

In the same approximation, the bandwidth Δf^i of the channel determines the spatial width

$$\Delta R^i = m_{e0}\pi \Delta f^i/(e\nabla B\sqrt{1 - k_B T^i_{Rad}/m_{e0}c^2}) \tag{2}$$

of the emission layer. No finite thickness of the emission layer is considered, which of course has to be done in a closer approach. Generally location and resolution can be defined as follows. Assuming the spectrally and spatially resolved ECE intensity distribution $\partial^2 I/\partial f \partial R$, is known, then the integral

$$dI^i/dR = \int_0^{+\infty} (\partial^2 I/\partial f \partial R) H^i df \tag{3}$$

defines the spatially resolved intensity distribution along the line of sight for the ith filter with normalized transmission function $H^i(f)$. From equation (3) the avarage location

$$< R^i >= \int_{-\infty}^{+\infty} R(dI^i/dR)dR / \int_{-\infty}^{+\infty} (dI^i/dR)dR \tag{4}$$

is assigned to the ith filter as the position of the emission layer. Furthermore the mean square deviation $< (\Delta R^i)^2 >$ from $< R^i >$ is determined. Then the spatial width of the emission layer can be defined by

$$\Delta R^i = 2\sqrt{< (\Delta R^i)^2 >} \quad . \tag{5}$$

In case dI^i/dR has a Gaussian shape, 68.3 % of the intensity, collected by the ith filter, is emitted between $R^i - \sqrt{< (\Delta R^i)^2 >}$ and $R^i + \sqrt{< (\Delta R^i)^2 >}$. For an individual ECE frequency these definitions are appropriate to evaluate the width of the emission layer for one spectral component, i.e. the 'natural width'.

Application to W7-X conditions

The ECE intensity distribution $\partial^2 I/\partial f \partial R$ is evaluated with the ray-tracing code TRAVIS for the W7-X standard configuration. In order to present in a first step basic features of the localisation and spatial resolution, constant n_e and T_e profiles are assumed along the sightline. Subsequently the approach is applied for a realistic case with n_e and T_e profiles, as gained by a predictive transport modelling code [5]. The ray-tracing code TRAVIS provides the ECE spectrum, emitted by the plasma, and the corresponding radiation temperature T_{Rad}, considering the radiation transfer equation [6,7]. The plasma emissivity and the absorption along a given line of sight are evaluated, determining the spectrally and spatially resolved ECE intensity. For TRAVIS the relevant input parameters are besides the ECE sightline the magnetic configuration of W7-X and the electron density and temperature profiles.

For constant electron density (n_e=5×10^{19} m^{-3}) and constant electron temperature profile (T_e=1 keV, 5 keV or 10 keV), the ECE intensity distribution $\partial^2 I/\partial f \partial r_{eff}$ is evaluated with TRAVIS. The result is shown in figure 1. As expected, due to the relativistic down-shift, the emission layer for a given frequency lies behind the cold resonance location. The transmission function $H^i(f)$ of each radiometer filter is assumed to be of rectangular shape and is represented by a set of 11 frequencies within the filter passband. Applying the definition of localisation (eq. (4)), the evaluation shows, that the emission layer moves away from the cold resonance location into the direction of increasing magnetic field, beeing 4 cm for T_e=10 keV (fig. 1b). The emission layer widths for individual frequencies and for radiometer filters are almost independent on frequency, but increase with T_e (fig. 1c). For low T_e the instrumental filter bandwidths Δf^i mainly determine the width of emission detected approaching the 'natural width' limit

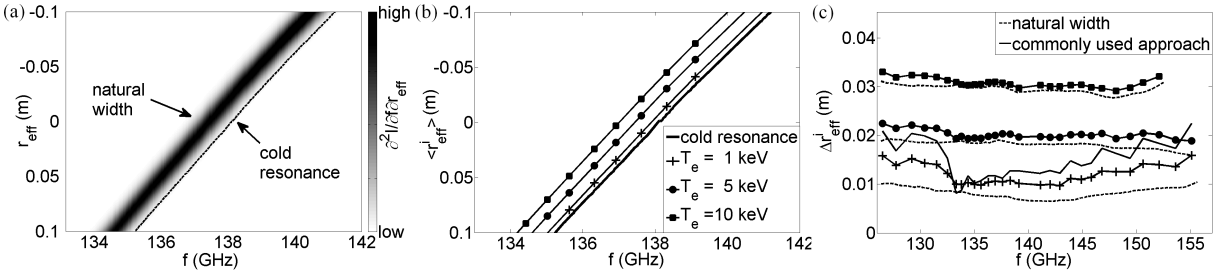

Figure 1: Localisation and spatial resolution of ECE diagnostics for standard configuration of W7-X, line of sight of standard ECE diagnostics, constant electron density profile n_e=5×10^{19} m^{-3} and one of three constant temperature profiles T_e=1 keV, 5 keV or 10 keV. (a) Spectrally and spatially resolved ECE intensity distribution $\partial^2 I/\partial f \partial r_{eff}$ (gray scale) evaluated by TRAVIS for constant electron temperature profile (T_e=5 keV). For clearness the spatial scale (ordinate) is reversed. For a given frequency the emission layer is localised behind the cold resonance (black dashed). (b) Position of emission layer $< r^i_{eff} >$. The distance of $< r^i_{eff} >$ (solid with symbols) to the cold resonance location (solid) increases with T_e. (c) Emission layer width Δr^i_{eff} for radiometer channels (same legend as in fig. 1b) and individual frequencies ('natural width').

for high T_e. For vanishing T^i_{Rad} the commonly used approach (eq. (2)) gives widths independent on T_e, varying between 1-2 cm.

To gain the ECE intensity distribution from TRAVIS for more realistic conditions a peaked T_e-profile with $T_e(0)$=6.39 keV (fig. 2a) as determined from transport modelling has been used (ECRH 4 MW, β = 0.02, $n_e(0)$=8×10^{19} m^{-3}). In addition to the intensity distribution, the ECE intensity spectrum in terms of T_{Rad} is retrieved from TRAVIS (fig. 2b). For the determination of the T_e profile only the frequency range 127-159 GHz is of interest. In the plasma core the emission layer is located 2 cm behind the cold resonance (fig. 3a). The emission layer widths for individual frequencies and filters change strongly between 1 cm and 3.5 cm (fig. 3b). In a narrow frequency window around 128 GHz an increase of the width for individual frequencies to 3.5 cm is present caused by the small ∇B at r_{eff}=0.4 m (fig. 2c), due to finite beta effects. Because of the magnetic field gradient increase below r_{eff}=0.4 m, the width drops. Since T_e increases and ∇B is not that steep in the range from 0 m< r_{eff} <0.4 m, the width increases again above 130 GHz. The radiation temperature approaches the maximum in the plasma

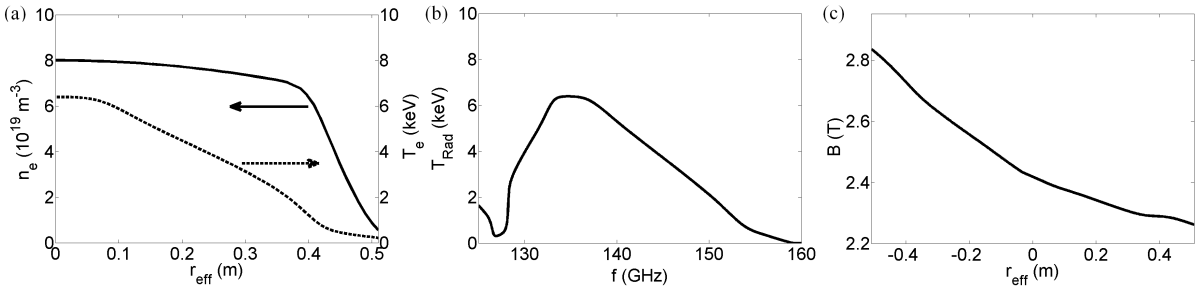

Figure 2: Plasma parameter for W7-X standard configuration and normalized plasma pressure β=0.02. (a) Flat electron density and peaked temperature profile, resulting from transport simulation for central ECRH heating of 4 MW. (b) Radiation temperature T_{Rad} for realistic n_e and T_e profile (fig. 2b) evaluated with TRAVIS. For the determination of the T_e profile only the spectral range 127-159 GHz is relevant. The plasma is optically thin for frequencies below 127 GHz reflecting strongly down-shifted ECE from the plasma center. (c) Magnetic field B along line of sight for LFS ECE diagnostic. The ECE line of sight is crossed by the last closed flux surface (LCFS) at the effect radius r_{eff}=-0.51 m (HFS) and r_{eff}=0.51 m (LFS).

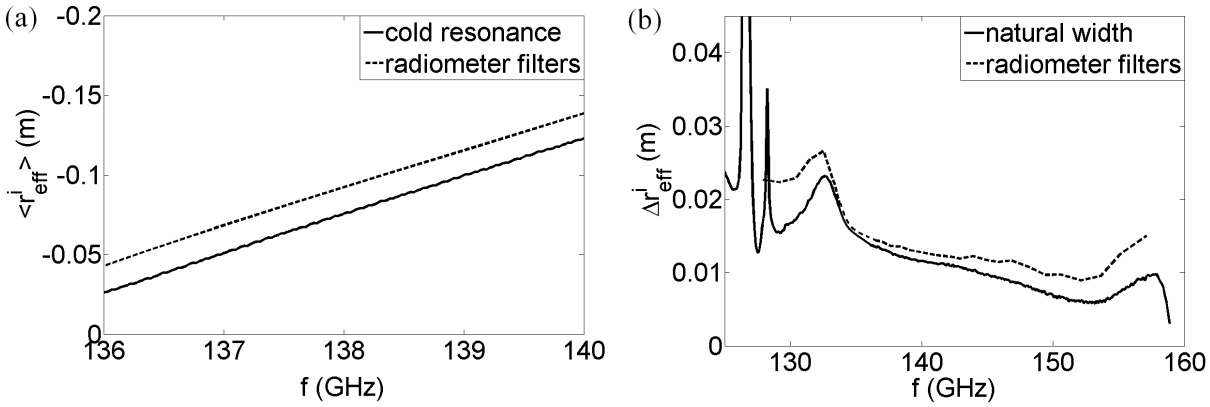

Figure 3: Localisation and spatial resolution for standard ECE diagnostics (radiometer filters) for realistic conditions at W7-X. (a) Emission layer position $< r^i_{eff} >$. In the plasma center, the distance from $< r^i_{eff} >$ (dashed) to the cold resonance (solid) is about 2 cm. (b) Emission layer width Δr^i_{eff} (dashed). In comparison the emission layer width for individual frequencies (solid) is given.

center, where a ∇B increase is evident, yielding a second maximum (at around 132 GHz). In the range 133-152 GHz the widths decrease strongly to values below 1 cm, due to raising ∇B and decreasing T_e. At even higher frequencies a small peak occurs, caused by the reduced optical depth due to the drop of n_e at the very edge of the plasma. Close to 159 GHz a strong decrease is evident due to the vanishing temperature at the plasma edge.

3 Conclusion

An advanced approach was introduced, to localise the radiation temperature, measured by a multi-channel radiometer. Furthermore, the spatial width of the emission layer is stated for a given radiometer channel transmission and for an individual frequency. To apply this approach, knowledge of the ECE intensity distribution, spectrally and spatially resolved, is obligatory. With the ray-tracing code TRAVIS, the ECE intensity distribution is determined. The approach is demonstrated for the low-field-side ECE diagnostics and standard configuration of W7-X for two sets of conditions. The approach gives an emission layer displacement of a few centimeters away from the cold resonance. The width of the emission layer broadens for increasing T_e. For the experimental conditions studied the interplay of ∇B, n_e and T_e profile causes a variation of the emission layer width (1-3.5 cm) with frequency displaying three explainable peaks in the relevant frequency range.

4 References

[1] S. Schmuck et al., Fusion Eng. Des. **84**, 1739 (2009)
[2] H. J. Hartfuss et al., Plasma Phys. Control. Fusion **39**, 1693 (1997)
[3] Ch. Fuchs et al., Rev. Sci. Instrum. **72**, 383 (2001)
[4] N. B. Marushchenko et al., Fusion Sci. Technol. **50**, 395 (2006)
[5] Y. Turkin et al., Fusion Sci. Technol. **50**, 387 (2006)
[6] N. B. Marushchenko et al., Proc. 14th Joint Workshop Electron Cyclotron Heating (Santorini, Greece, 9-12 May 2006)
[7] N. B. Marushchenko et al., Proc. 16th Toki Conf. (Toki, Japan, 5-8 December 2006)